

Efficient algorithm for asymptotics-based configuration-interaction methods and electronic structure of transition metal atoms

Christian B. Mendl^{1,a)} and Gero Friesecke^{1,a)}¹Center for Mathematics, TU Munich, Garching 85748, Germany

(Received 19 April 2010; accepted 7 September 2010; published online 8 November 2010)

Asymptotics-based configuration-interaction (CI) methods [G. Friesecke and B. D. Goddard, *Multiscale Model. Simul.* **7**, 1876 (2009)] are a class of CI methods for atoms which reproduce, at fixed finite subspace dimension, the exact Schrödinger eigenstates in the limit of fixed electron number and large nuclear charge. Here we develop, implement, and apply to *3d* transition metal atoms an efficient and accurate algorithm for asymptotics-based CI. Efficiency gains come from exact (symbolic) decomposition of the CI space into irreducible symmetry subspaces at essentially linear computational cost in the number of radial subshells with fixed angular momentum, use of reduced density matrices in order to avoid having to store wave functions, and use of Slater-type orbitals (STOs). The required Coulomb integrals for STOs are evaluated in closed form, with the help of Hankel matrices, Fourier analysis, and residue calculus. Applications to *3d* transition metal atoms are in good agreement with experimental data. In particular, we reproduce the anomalous magnetic moment and orbital filling of chromium in the otherwise regular series Ca, Sc, Ti, V, Cr. © 2010 American Institute of Physics. [doi:10.1063/1.3493677]

I. INTRODUCTION

The search for accurate computational methods for the *N*-electron Schrödinger equation at moderate computational cost has been a focus of activity for several decades.^{1–4} The present article is a contribution to one part of the picture, wave function methods for atoms. We develop, implement, and apply to transition metal atoms an algorithmic framework which renders asymptotics-based configuration-interaction (CI) computations for atoms with basis sets of up to 50 one-electron spin orbitals, up to 30 electrons, and full resolution of all valence electron correlations feasible. An attractive feature of our framework is that many steps are done *symbolically* by building on, systematizing, and automatizing the paper-and-pencil analysis of asymptotics-based CI for small atoms and minimal bases in Ref. 5. A MATLAB/MATHEMATICA implementation is available at Ref. 6.

CI methods^{3,7} approximate the electronic Schrödinger equation by projecting it onto a well chosen subspace spanned by Slater determinants. More precisely, the Schrödinger equation for an atom or ion with *N* electrons is

$$H\psi = E\psi, \quad \psi \in L_a^2\left(\left(\mathbb{R}^3 \times \left\{-\frac{1}{2}, +\frac{1}{2}\right\}\right)^N\right), \quad (1)$$

where *H* is the Hamiltonian of the system [see Eq. (3) below], ψ is the wave function, and *E* is the energy. The wave function $\psi = \psi(x_1, s_1, \dots, x_N, s_N)$ depends on the positions $x_i \in \mathbb{R}^3$ and spins $s_i \in \{-\frac{1}{2}, +\frac{1}{2}\}$ of all electrons and belongs to the space $L_a^2\left(\left(\mathbb{R}^3 \times \left\{-\frac{1}{2}, +\frac{1}{2}\right\}\right)^N\right)$ of square-integrable, antisymmetric functions on $\left(\mathbb{R}^3 \times \left\{-\frac{1}{2}, +\frac{1}{2}\right\}\right)^N$. A CI method is an approximation of Eq. (1) by an equation of the form

$$PH\Psi = E\Psi, \quad \psi \in V \subset L_a^2\left(\left(\mathbb{R}^3 \times \left\{-\frac{1}{2}, +\frac{1}{2}\right\}\right)^N\right) \quad (2)$$

P = orthogonal projector onto *V*,

where *V* is a span of a finite number of Slater determinants $|\chi_{i_1}, \dots, \chi_{i_N}\rangle$ built from a finite number of spin orbitals $\{\chi_1, \dots, \chi_K\} \subset L^2(\mathbb{R}^3 \times \{-\frac{1}{2}, +\frac{1}{2}\})$. We recall the well known *fundamental difficulty of CI methods*: Eq. (1) is a partial differential equation in very high space dimension, e.g., dimension 72 in case of a single chromium atom as treated in this paper. Hence, when discretizing the single-electron state space by a reasonable number of spin orbitals, $L^2(\mathbb{R}^3 \times \{-\frac{1}{2}, +\frac{1}{2}\}) \approx \text{Span}\{\chi_1, \dots, \chi_K\}$, the ensuing natural choice $V = \text{span}\{|\chi_{i_1} \dots \chi_{i_N}\rangle : 1 \leq i_1 < \dots < i_N \leq K\}$ (full CI) has a prohibitively large dimension, $\binom{K}{N}$.

Our principal contribution here is the development of an efficient algorithm that minimizes the curse of dimension. The main savings come from exact (i.e., symbolic) and efficiently automated exploitation of symmetry to perform dimension reduction. Other ingredients are the use of reduced density matrices in order to avoid having to store wave functions and the use of Slater-type orbitals (STOs) including exact orthonormalization and Coulomb integral evaluation. The algorithm has been implemented for a recent variant of CI, asymptotics-based CI,⁵ which exploits the asymptotic results in Ref. 8 and has the attractive features that the CI subspace, if its dimension is *K*, reproduces correctly the first *K* Schrödinger eigenstates in the limit of fixed *K*, fixed electron number, and large nuclear charge *Z*. [This limit, which has a large literature (see, in particular, Refs. 9 and 10), captures the physical environment of inner shell electrons, and has the *multiscale* property that the ratio of the first spectral gap to the ground state energy of the Schrödinger equation tends to zero,⁵ with the experimental ratio for true

^{a)}Authors to whom correspondence should be addressed. Electronic addresses: gf@ma.tum.de and christian_mendl@hotmail.com

atoms being very close to zero, about 1 part in 1000 for carbon and oxygen and 1 part in 30 000 for Cr and Fe.] The main part of the algorithm, automated symmetry reduction, can be easily adapted to other CI methods and orbitals (such as Gaussians).

As a typical application, we treat here the transition metal series Ca, Sc, Ti, V, Cr, modeled by 18 core electrons occupying Slater orbitals of type $1s$ to $3p$, and an active space consisting of $3d$, $4s$, $4p$, and $4d$ Slater orbitals (of either spin) accommodating the two to six valence electrons. The resulting CI space V for Cr has dimension $d = \binom{28}{6} = 376\,740$, and the CI Hamiltonian has $d(d+1)/2 \approx 7 \times 10^{10}$ entries. But automated symmetry reduction shows (see Table III) that only 14 basis functions contribute to the experimental ground state configuration and symmetry, $[\text{Ar}]4s^1 3d^5 \ ^7S$, allowing to evaluate the ensuing eigenvalues and eigenstates easily and to machine precision. Our results, detailed in Sec. VII below, provide an *ab initio* explanation of the anomalous magnetic moment of chromium (experimentally, the ground state has six instead of the expected four aligned spins) and the underlying anomaly in the filling order of $3d$ versus $4s$ orbitals in the semi-empirical orbital picture of the transition metal atoms (chromium, unlike its four predecessors Ca, Sc, Ti, and V, possesses only one instead of two $4s$ electrons). It is well known^{11–14} that single-determinant Hartree–Fock, relativistic Hartree–Fock, and density functional theory calculations (even with the best exchange–correlation functionals such as B3LYP) render the correct filling orders and ground state symmetries only for some but not all transition metal elements (see Sec. VII).

In the remainder of this section, we describe our algorithm for *exact (symbolic), efficient symmetry partitioning*. The (nonrelativistic, Born–Oppenheimer) Hamiltonian

$$H = \sum_{i=1}^N \left(-\frac{1}{2} \Delta_{\mathbf{x}_i} - \frac{Z}{|\mathbf{x}_i|} \right) + \sum_{1 \leq i < j \leq N} \frac{1}{|\mathbf{x}_i - \mathbf{x}_j|} \quad (3)$$

governing atoms/ions with N electrons and nuclear charge Z has the symmetry group

$$SU(2) \times SO(3) \times \mathbb{Z}_2, \quad (4)$$

consisting of simultaneous rotation of electron spins and simultaneous rotation and sign reversal of electron positions. This leads to the well known conservation law that the Hamiltonian leaves the simultaneous eigenspaces of the spin, angular momentum, and parity operators

$$L^2, L_z, S^2, S_z, \hat{R} \quad (5)$$

invariant (see Sec. II A for precise definitions of these operators). The fact that partitioning into symmetry subspaces significantly lowers computational costs has long been known to, and exploited by, theorists (see, e.g., Ref. 15). A striking example is the paper-and-pencil symmetry decomposition^{8,16} of a minimal asymptotics-based CI Hamiltonian *PHP* for the second-period atoms He to Ne, with active space consisting of the eight $2s$ and $2p$ spin orbitals accommodating the valence electrons. For carbon, there are four valence electrons, so the active space has dimension $\binom{8}{4} = 70$ and the CI Hamiltonian is a 70×70 matrix. But due to symmetry it decom-

poses into fifteen 2×2 blocks and forty 1×1 blocks.

The main algorithmic steps which automate such decompositions are as follows.

- One starts by partitioning the CI space into configurations, i.e., subspaces such as $1s^{n_1} 2s^{n_2} 2p^{n_3} \dots$ with a fixed number n_i of electrons in each subshell (see Sec. II B below). It suffices to symmetry-decompose each configuration because the symmetry group, unlike the Hamiltonian, leaves each configuration invariant individually.
- Each configuration is isomorphic to a *non-antisymmetrized* tensor product of lower-dimensional factors. The tensor factors consist of single $1s, 2s, 2p, \dots$ subshells (see Sec. II B). This product structure is essential for step (d) below.
- The splitting up of each factor into simultaneous eigenspaces of the symmetry operators (5) is done via a suitable algorithm from the mathematics literature for simultaneous diagonalization of commuting matrices, for instance, that of Bunse-Gerstnert, Byers, and Mehrmann.¹⁷ (We are indebted to Folkmar Bornemann for helpful advice regarding this step.) Exact eigenstates are recovered from the numerical eigenstates through exploiting that the squares of the eigenstate coefficients are, by representation theory, rational numbers.
- Given simultaneous eigenstates of the symmetry operators for each factor, simultaneous eigenstates of a two-factor tensor product are known explicitly in terms of the well known Clebsch–Gordan coefficients, and those for a many-factor tensor product are easily obtained by iteration of the Clebsch–Gordan formulae. This yields the desired decomposition of each configuration.

A key feature of the algorithms (a)–(d) is the computational cost grows only *linearly* with the number of subshells, provided the angular momentum cutoff is held fixed. Thus, say, the cost of including s orbitals of type $1s, 2s, \dots, ns$ is only $\mathcal{O}(n)$ (see Sec. VI).

The structure of this paper is as follows. In Sec. II we briefly review asymptotics-based CI. Section III contains the main contribution of this paper, namely, exact reduction steps leading to significant savings of computational time and memory storage. In Sec. IV we treat orthonormalization and Coulomb integral evaluation for general atomic Slater-type orbitals. We summarize all algorithmic steps in Sec. V and carefully estimate the costs in Sec. VI. Finally, in Sec. VII we apply the algorithmic framework to the electronic structure of potassium, calcium, and the transition metals scandium to zinc.

II. ASYMPTOTICS-BASED CI

We briefly recall the setup and features relevant to the present work, referring to Refs. 5 and 16 for further information.

A. Symmetries

Due to invariance of the Hamiltonian (3) under the symmetry group (4), the set of operators (5) commutes with the Hamiltonian and with each other, for arbitrary N and Z . These operators play an important role in our algorithmic framework. Here and below we use the standard notation $L = \sum_{i=1}^N L(i)$ (many-body angular momentum operator), $L(i) = \mathbf{x}_i \wedge \mathbf{i}^{-1} \nabla_{\mathbf{x}_i}$ (angular momentum operator acting on the position coordinates $\mathbf{x}_i \in \mathbb{R}^3$ of the i th electron), L_x, L_y, L_z (components of L), and analogously for spin (see, e.g., Ref. 16). The parity operator $\psi(\mathbf{x}_1, s_1, \dots, \mathbf{x}_N, s_N) \mapsto \psi(-\mathbf{x}_1, s_1, \dots, -\mathbf{x}_N, s_N)$ is denoted by \hat{R} .

B. Configurations

Our treatment of symmetry reduction is independent of the particular orbitals used and works within the context of general N -electron configurations as introduced in Ref. 5, definition 2.2: Let

$$V_1, V_2, \dots \subset L^2(\mathbb{R}^3 \times \{-\frac{1}{2}, +\frac{1}{2}\}) \quad (6)$$

be any collection of mutually orthogonal subspaces of the single-electron Hilbert space, which are irreducible representation spaces for the joint spin and angular momentum algebra $\text{span}\{L_x, L_y, L_z, S_x, S_y, S_z\}$ [or, equivalently, which are joint eigenspaces of L^2 and S^2 with minimal dimension $(2\ell+1)(2s+1)$ given the respective eigenvalues $\ell(\ell+1)$ and $s(s+1)$]. Then, a configuration of an N -electron atom or ion is a subspace of the antisymmetrized N -electron state space $L_a^2((\mathbb{R}^3 \times \{-\frac{1}{2}, +\frac{1}{2}\})^N)$ of the following form:

$$\begin{aligned} \mathcal{C}^{d_1, \dots, d_k} &= \text{span}\{|\chi_1, \dots, \chi_N\rangle : \{\chi_1, \dots, \chi_N\} \\ &\text{any orthonormal set in } L^2(\mathbb{R}^3 \times \{-\frac{1}{2}, +\frac{1}{2}\}) \\ &\text{with } \#\{i: \chi_i \in V_j\} = d_j\}, \end{aligned}$$

where $(d_1, \dots, d_k) = \mathbf{d}$ is a partition of N (i.e., $0 \leq d_j \leq \dim V_j$, $\sum_j d_j = N$). Physically, the V_j are subshells and the d_j are occupation numbers. The main point is that all choices of the χ_i 's consistent with the requirement that a fixed number of them have to be picked from each V_j have to be included.

Configurations, unlike general subspaces of $L_a^2((\mathbb{R}^3 \times \{-\frac{1}{2}, +\frac{1}{2}\})^N)$ spanned by a basis of Slater determinants, are invariant under the symmetry group (4) and its generators L , S , and \hat{R} , and in particular under the operators (5). The same holds for multiconfiguration subspaces

$$V = \text{span}\{\mathcal{C}^{d^{(1)}}, \dots, \mathcal{C}^{d^{(M)}}\}, \quad (7)$$

where each $\mathcal{C}^{d^{(i)}}$ is a configuration.

C. Asymptotics-based selection of configurations

Equation (7) still leaves a great deal of freedom for the precise specification of the CI subspace V . In asymptotics-based CI,⁵ the traditional step of an intermediate Hartree–Fock calculation to determine orbitals is replaced by the theoretical requirement that the ansatz space reproduce correctly the lowest Schrödinger eigenstates in the isoelectronic limit

$Z \rightarrow \infty$ (see Theorem 1 below). This requires STOs instead of the asymptotically inexact linear combinations of Gaussians, which are common in molecular calculations and corresponds to full CI in an active space for the valence electrons (instead of truncating valence electron correlations in terms of order of excitation with respect to a reference determinant as in double-excited CI or nonlinearly approximating them as in coupled cluster theory).

Asymptotics-based CI preserves the spin and angular momentum symmetries of the original Hamiltonian, and obeys the virial theorem, by determining orbital dilation parameters self-consistently for the actual CI wave functions instead of precomputing them via a Hartree–Fock calculation. (The fact that methods with self-consistent dilation parameters always obey the virial theorem was pointed out by Löwdin.¹⁸)

The specific asymptotics-based CI model for atoms used in this paper is as follows.

- (A) (Choice of a parametrized, asymptotically exact family of subspaces) We specify the orbital spaces in Eq. (6) as

$$V_{n\ell}^Z := \text{Span}\{\psi_{n\ell m \uparrow}, \psi_{n\ell m \downarrow}\}_{m=-\ell \dots \ell},$$

$$n = 1, 2, \dots, \quad \ell = 0, \dots, n-1,$$

with orthonormal Slater (or hydrogen-like) orbitals

$$\psi_{n\ell m}(\mathbf{x}) = r^\ell Y_{\ell m}(\vartheta, \varphi) p_{n\ell}(Z_{1\ell}, \dots, Z_{n\ell}, r) e^{-Z_{n\ell} r},$$

$r = |\mathbf{x}|$, and polynomials $p_{n\ell}(Z_{1\ell}, \dots, Z_{n\ell}, \cdot)$ of order $n - \ell - 1$ [see Eq. (21)]. Here, $\mathbf{Z} = (Z_{1,0}, Z_{2,0}, Z_{2,1}, \dots)$ is a vector of dilation parameters $Z_{n\ell} > 0$. We then set

$$V^Z := \text{span}\left\{ \bigcup_{\mathbf{d} \in \mathcal{D}} \mathcal{C}^{\mathbf{d}} \right\},$$

where $\mathbf{d} = (d_{n\ell})$, $n = 1, 2, \dots$, $\ell = 0, \dots, n-1$ is a vector of occupation numbers which sum to N , and \mathcal{D} is a finite set of such vectors such that

- (i) $0 \leq d_{n\ell} \leq \dim V_{n\ell}^Z = 2 \cdot (2\ell + 1)$.

Prototypical is the set \mathcal{D} consisting of all configurations such that, with respect to alphabetical ordering of the indices (n, ℓ) ,

- (ii) $d_{n\ell} = 0$ for $(n, \ell) > (n, \ell)_{\max}$
 (iii) $d_{n\ell} = 2 \cdot (2\ell + 1)$ for $(n, \ell) \leq (n, \ell)_{\min}$.

Here, (ii) is a cutoff condition and (iii) says that all subshells up to $(n, \ell)_{\min}$ are completely filled.

- (B) (Subspace eigenvalue problem) For each symmetry subspace

$$V_{\ell sp}^Z := \{\psi \in V^Z : L^2 \psi = \ell(\ell + 1)\psi,$$

$$S^2 \psi = s(s + 1)\psi, \quad \hat{R} \psi = p\psi\}$$

of V^Z (angular momentum, spin, and parity quantum numbers ℓ , s , and p , respectively), $E_j^{\text{CI}, Z} :=$ eigenvalues of $P^Z H P^Z$ on $V_{\ell sp}^Z$, $\psi_j^{\text{CI}, Z} :=$ corresponding orthonormal eigenstates, where $P^Z =$ orthogonal projector of $L_a^2((\mathbb{R}^3 \times \{-\frac{1}{2}, +\frac{1}{2}\})^N)$ onto V^Z .

- (C) (Variational parameter determination) For each symmetry subspace $V_{\ell,sp}^Z \subset V^Z$, $Z_* := \operatorname{argmin}_Z (\min_j E_j^{\text{CI},Z})$, $E_j^{\text{CI}} := E_j^{\text{CI},Z_*}$, and $\psi_j^{\text{CI}} := \psi_j^{\text{CI},Z_*}$.

Here $\operatorname{argmin}_x f(x)$ denotes a minimizer of the functional f . We remark that minimizing dilation parameters Z are expected to exist provided the nuclear charge Z is greater or equal to the number N of electrons (in which case the full Rayleigh–Ritz variational principle possesses a minimizer¹⁹). In our numerical computations, we always found this to be the case.

Also, for future reference we define

$$\begin{aligned} c^{\text{CI}} &:= \text{number of core spin-orbitals of the CI model} \\ &= \sum_{(n,\ell) \leq (n,\ell)_{\min}} 2(2\ell + 1), \end{aligned}$$

$$\begin{aligned} t^{\text{CI}} &:= \text{total number of spin-orbitals of the CI model} \\ &= \sum_{(n,\ell) \leq (n,\ell)_{\max}} 2 \cdot (2\ell + 1). \end{aligned}$$

Of course, the model only makes sense (i.e., the space V is nonempty), provided the cutoffs $(n,\ell)_{\min}$ and $(n,\ell)_{\max}$ are chosen so that $c^{\text{CI}} \leq N \leq t^{\text{CI}}$.

We summarize the asymptotic properties of the above model in the following straightforward generalization of Theorem 2.1 in Ref. 5 on second-period atoms. The following numbers associated with the noninteracting N -electron atom play a role: $n_-(N)$, $n_+(N)$, $c(N)$, and $t(N)$, which denote the number of closed shells, closed or open shells, core spin-orbitals, and core or valence spin-orbitals, respectively. Explicitly,¹⁶ n_- and n_+ can be expressed in terms of the number of spin orbitals in the first n' hydrogen shells, $f(n') := \sum_{n=1}^{n'} \sum_{\ell=0}^{n-1} 2 \cdot (2\ell + 1)$, as the largest integer such that $f(n_-) < N$, respectively, the smallest integer such that $f(n_+) \geq N$. One then has $c(N) = f(n_-(N))$ and $t(N) = f(n_+(N))$.

Theorem 1. (Correct asymptotic behavior) The CI model (A), (B), and (C) with \mathcal{D} given by (ii) and (iii) has the following properties. In the large nuclear charge limit $Z \rightarrow \infty$ for N and $\dim V^Z$ fixed, the lowest

$$\left(\begin{array}{c} \min(t(N), t^{\text{CI}}) - \max(c(N), c^{\text{CI}}) \\ N - \max(c(N), c^{\text{CI}}) \end{array} \right)$$

eigenvalues $E_1^{\text{CI}} \leq E_2^{\text{CI}} \leq \dots$ and $E_1 \leq E_2 \leq \dots$ (repeated according to multiplicity) of the CI model, respectively, the Schrödinger equation (1) satisfy

$$\lim_{Z \rightarrow \infty} \frac{E_j^{\text{CI}}}{E_j} = 1.$$

If moreover $c^{\text{CI}} \leq c(N)$ (i.e., the CI model does not constrain the occupation numbers of any noncore orbitals) and $t^{\text{CI}} \geq t(N)$ (i.e., at least all core and valence orbitals are included in the CI model), then there exist orthonormal CI, respectively, Schrödinger eigenstates ψ_i^{CI} and ψ_i corresponding to the above eigenvalues such that

$$\lim_{Z \rightarrow \infty} \|\psi_i^{\text{CI}} - \psi_i\| = 0,$$

where $\|\cdot\|$ is the norm on the N -electron space $L_a^2(\mathbb{R}^3 \times \{-\frac{1}{2}, +\frac{1}{2}\})^N$.

Finally, under the same condition on c^{CI} and t^{CI} , the spectral gaps satisfy

$$\lim_{Z \rightarrow \infty} \frac{\Delta E_j^{\text{CI}}}{\Delta E_j} = 1 \quad (8)$$

whenever $\Delta E_j > 0$, where $\Delta E_j^{\text{CI}} = E_j^{\text{CI}} - E_1^{\text{CI}}$ and $\Delta E_j = E_j - E_1$ ($j \geq 2$).

We emphasize that the above theorem only covers the regime of large Z . For neutral atoms, the highest eigenstates in the ansatz space of asymptotics-based CI are typically observed to lie above higher Rydberg states or even above the bottom of the continuous spectrum.

III. EXACT REDUCTION STEPS AND LS DIAGONALIZATION

This section explains exact reduction steps which are essential for cutting down the calculation time and storage requirement of the algorithmic implementation.

A. Tensor product structure of configurations

Our first observation connects N -particle configurations (see Sec. II B) to the nonantisymmetrized tensor product of antisymmetrized d_j -particle states, preserving the action of the angular momentum and spin operators. Here and below, we use the standard notation²⁰ $\wedge^n V$ for the n -fold antisymmetrized tensor product of a vector space V and $V \otimes W$ for the tensor product of two spaces V and W .

Proposition 2: Consider irreducible representation spaces V_1, \dots, V_k as in Eq. (6) and particle numbers $d_1, \dots, d_k \geq 0$. Then the following isometric isomorphism holds:

$$\mathcal{C}^{d_1, \dots, d_k} \cong \bigotimes_{j=1}^k \wedge^{d_j} V_j. \quad (9)$$

A canonical mapping of basis vectors is given by

$$\mathcal{T}: |\chi_1^1, \dots, \chi_{d_1}^1, \dots, \chi_1^k, \dots, \chi_{d_k}^k\rangle \mapsto |\chi_1^1, \dots, \chi_{d_1}^1\rangle \otimes \dots \otimes |\chi_1^k, \dots, \chi_{d_k}^k\rangle,$$

with $\chi_i^j \in V_j$ for all i, j . Moreover, \mathcal{T} commutes with the action of the angular momentum and spin operators, i.e.,

$$\mathcal{T}(\mathbf{L}\psi) = \left(\sum_{j=1}^k \mathbf{L}_j \right) \mathcal{T}(\psi), \quad \mathcal{T}(\mathbf{S}\psi) = \left(\sum_{j=1}^k \mathbf{S}_j \right) \mathcal{T}(\psi)$$

for all $\psi \in \mathcal{C}^{d_1, \dots, d_k}$, where \mathbf{L}, \mathbf{S} on the left hand sides are N -particle operators and each $\mathbf{L}_j, \mathbf{S}_j$ on the right hand side acts on the d_j -particle tensor factor $\wedge^{d_j} V_j$.

Proof: Clear from the definitions.

In particular, $\dim(\mathcal{C}^{d_1, \dots, d_k}) = \prod_j \binom{\dim(V_j)}{d_j}$. Note that Eq. (9) inherently takes into account the antisymmetrization of fermionic wave functions without requiring any additional normalization factors. The isometry (9) is reflected in the algorithmic implementation by ordering Slater determinants lexicographically and arranging coefficients accordingly, see Fig. 1.

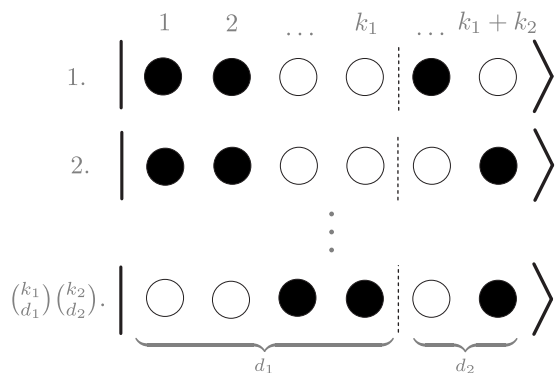


FIG. 1. Lexicographical ordering of the $\binom{k_1}{d_1} \binom{k_2}{d_2}$ Slater determinants restricted to a fixed configuration involving two one-particle subspaces V_1 and V_2 of dimensions k_1 and k_2 , with d_1 particles in orbitals $1, \dots, k_1$ and d_2 particles in the remaining orbitals $k_1 + 1, \dots, k_1 + k_2$. Filled circles correspond to filled orbitals. Usefully, restriction to a configuration preserves lexicographical ordering.

B. LS diagonalization

A priori, the diagonalization of the angular momentum and spin (LS) operators seems as expensive as diagonalizing the Hamiltonian itself, yet it turns out to come at much cheaper costs. It involves mostly algebra and can be done prior to setting up the Hamiltonian.

- (1) Calculate all irreducible LS eigenspaces for each many-particle subshell. In more detail, let $u = s, p, d, \dots$ denote the angular momentum subshells in common chemist's notation and set

$$V_u := \text{span}\{Y_{\ell m \uparrow}, Y_{\ell m \downarrow}\}_{\ell = \text{ang}(u), m = -\ell \dots \ell}$$

with the spherical harmonics $Y_{\ell m}$. Note that this is an explicit realization of the spaces in Eq. (6). Then, for all $n = 1, \dots, \dim(V_u)$ (equal to $2 \times (2\ell + 1)$), decompose the n -particle space $\wedge^n V_u$ into the direct sum of irreducible spin and angular momentum representation spaces. That is,

$$\wedge^n V_u = \bigoplus_i V_{uni} \quad (10)$$

such that

$$L^2 \varphi = \ell_i(\ell_i + 1) \varphi,$$

$$S^2 \varphi = s_i(s_i + 1) \varphi \quad \forall \varphi \in V_{uni},$$

$$\dim(V_{uni}) = (2\ell_i + 1)(2s_i + 1).$$

Explicit results are shown in Table I; subshells from $\wedge^4 V_d$ to $\wedge^{10} V_d$ are omitted for brevity's sake and only states with maximal L_z and S_z quantum numbers are displayed; applying the ladder operators $L_- = L_x - iL_y$ and $S_- = S_x - iS_y$ yields the remaining wave functions. Note that symmetry levels can appear twice within a many-particle subshell, e.g., 2D in $\wedge^3 V_d$. In concordance with the Clebsch–Gordan method below, the ordered single-particle orbitals are L_z and S_z eigenstates, denoted by

$$(s, \bar{s}) \quad \text{for } V_s,$$

$$(p_1, \bar{p}_1, p_0, \bar{p}_0, p_{n_1}, \bar{p}_{n_1}) \quad \text{for } V_p,$$

$$(d_2, \bar{d}_2, d_1, \bar{d}_1, \dots, d_{n_2}, \bar{d}_{n_2}) \quad \text{for } V_d.$$

The highest quantum number appears first and $\bar{\cdot}$ equals spin down \downarrow (convention as in Ref. 16).

The decomposition (10) first requires a matrix representation of the angular momentum and spin operators $L_x, L_y, L_z, S_x, S_y, S_z$ on $\wedge^n V_u$. We obtain it by starting from the canonical single-particle representation on V_u (spherical harmonics) and writing the n -body operator in the form $B = \sum_{i,j} b_{ij} a_i^\dagger a_j$, where b_{ij} are the coefficients of the single-particle representation and a_i^\dagger and a_j are fermionic creation and annihilation operators. The operators $a_i^\dagger a_j$ map Slater determinants to Slater determinants; thus, all entries of their corresponding matrix representation are 0 or ± 1 .

The next task to arrive at Eq. (10) involves the simultaneous diagonalization of the pairwise commuting operators L^2, S^2, L_z, S_z . We present two alternatives.

Alternative 1

apply an algorithm of choice, e.g., Ref. 17, for the simultaneous diagonalization of L^2, S^2, L_z, S_z on $\wedge^n V_u$, denoting the eigenvalues or “quantum numbers” of L^2, S^2, L_z, S_z by $\ell(\ell+1), s(s+1), m_\ell, m_s$, respectively

```

for each subspaces  $W$  with  $m_\ell = \ell$  and  $m_s = s$  do
  choose an ONB  $\{\varphi_1, \dots, \varphi_r\}$  of  $W$ 
  for  $j = 1, \dots, r$  do
    add  $V_{unj} := \text{Span}\{\varphi_j, L_- \varphi_j, S_- \varphi_j, L_- S_- \varphi_j, \dots\}$  to the decomposition (10)
  end for
end for

```

Note that the iterative application of the ladder operators L_- and S_- ensures that the resulting subspaces V_{unj} are invariant irreducible representation spaces.

Alternative 2

count $\leftarrow 0$

```

for  $\ell = 0, 1, \dots$  and  $s = \begin{cases} \frac{1}{2}, \frac{3}{2}, \dots & n \text{ odd} \\ 0, 1, \dots & n \text{ even} \end{cases}$  do

```

$$X := (L^2 - \ell(\ell+1)\text{id}) (S^2 - s(s+1)\text{id}) (L_z - \ell\text{id}) (S_z - s\text{id})$$

calculate $W := \text{Kern}(XX^\dagger) \subset \wedge^n V_u$

if $W = \emptyset$ **then**

next for loop

end if

choose an ONB $\{\varphi_1, \dots, \varphi_r\}$ of W

for $j = 1, \dots, r$ **do**

add $V_{unj} := \text{Span}\{\varphi_j, L_- \varphi_j, S_- \varphi_j, L_- S_- \varphi_j, \dots\}$ to the decomposition (10)

end for

count \leftarrow count + r

stop if $\sum_{i=1}^{\text{count}} \dim(V_{uni}) = \dim(\wedge^n V_u)$

end for

The second alternative exchanges the direct diagonalization in alternative 1 for testing all potential eigenvalues (that is, integer or half-integer numbers) with $m_\ell = \ell$ and $m_s = s$. Efficient numerical methods exist for computing the kernel W , which take advantage of the sparse structure of the matrix representation.

- (2) Consider N -electron configurations $\mathcal{C}^{n_1, \dots, n_k}$ assembled

TABLE I. Irreducible LS eigenspace decompositions of $\wedge^n V_u$ in Eq. (10), showing states with maximal L_z and S_z quantum numbers only.

Configuration	Symmetry	L_z	S_z	Ψ
$\wedge^1 V_s$	2S	0	$\frac{1}{2}$	$ s\rangle$
$\wedge^2 V_s$	1S	0	0	$ s\bar{s}\rangle$
$\wedge^1 V_p$	$^2P^o$	1	$\frac{1}{2}$	$ p_1\rangle$
$\wedge^2 V_p$	1S	0	0	$1/\sqrt{3}(- p_1\bar{p}_{n1}\rangle + \bar{p}_1 p_{n1}\rangle + p_0\bar{p}_0\rangle)$
	3P	1	1	$ p_1 p_0\rangle$
	1D	2	0	$ p_1\bar{p}_1\rangle$
$\wedge^3 V_p$	$^4S^o$	0	$\frac{3}{2}$	$ p_1 p_0 p_{n1}\rangle$
	$^2P^o$	1	$\frac{1}{2}$	$1/\sqrt{2}(p_1\bar{p}_1 p_{n1}\rangle + p_1 p_0\bar{p}_0\rangle)$
	$^2D^o$	2	$\frac{1}{2}$	$ p_1\bar{p}_1 p_0\rangle$
$\wedge^4 V_p$	1S	0	0	$1/\sqrt{3}(- p_1\bar{p}_1 p_{n1}\bar{p}_{n1}\rangle - p_1 p_0\bar{p}_0 p_{n1}\rangle + \bar{p}_1 p_0\bar{p}_0 p_{n1}\rangle)$
	3P	1	1	$ p_1\bar{p}_1 p_0 p_{n1}\rangle$
	1D	2	0	$ p_1\bar{p}_1 p_0\bar{p}_0\rangle$
$\wedge^5 V_p$	$^2P^o$	1	$\frac{1}{2}$	$ p_1\bar{p}_1 p_0\bar{p}_0 p_{n1}\rangle$
$\wedge^6 V_p$	1S	0	0	$ p_1\bar{p}_1 p_0\bar{p}_0 p_{n1}\bar{p}_{n1}\rangle$
$\wedge^1 V_d$	2D	2	$\frac{1}{2}$	$ d_2\rangle$
$\wedge^2 V_d$	1S	0	0	$1/\sqrt{5}(d_2\bar{d}_{n2}\rangle - \bar{d}_2 d_{n2}\rangle - d_1\bar{d}_{n1}\rangle + \bar{d}_1 d_{n1}\rangle + d_0\bar{d}_0\rangle)$
	3P	1	1	$1/\sqrt{5}(-\sqrt{2}\cdot d_2\bar{d}_{n1}\rangle + \sqrt{3}\cdot d_1\bar{d}_0\rangle)$
	1D	2	0	$1/\sqrt{7}(-\sqrt{2}\cdot d_2\bar{d}_0\rangle + \sqrt{2}\cdot \bar{d}_2 d_0\rangle + \sqrt{3}\cdot d_1\bar{d}_1\rangle)$
	3F	3	1	$ d_2\bar{d}_1\rangle$
	1G	4	0	$ d_2\bar{d}_2\rangle$
$\wedge^3 V_d$	2P	1	$\frac{1}{2}$	$1/\sqrt{210}(4\sqrt{3}\cdot d_2\bar{d}_1\bar{d}_{n2}\rangle - 2\sqrt{3}\cdot d_2\bar{d}_1 d_{n2}\rangle - 4\sqrt{2}\cdot d_2\bar{d}_0\bar{d}_{n1}\rangle - \sqrt{2}\cdot d_2\bar{d}_0 d_{n1}\rangle - 2\sqrt{3}\cdot d_2\bar{d}_1 d_{n2}\rangle + 5\sqrt{2}\cdot d_2\bar{d}_0 d_{n1}\rangle + 3\sqrt{3}\cdot d_1\bar{d}_1 d_{n1}\rangle + 3\sqrt{3}\cdot d_1\bar{d}_0 d_0\rangle)$
	4P	1	$\frac{3}{2}$	$\frac{1}{\sqrt{5}}(-\sqrt{3}\cdot d_2\bar{d}_1 d_{n2}\rangle + \sqrt{2}\cdot d_2\bar{d}_0 d_{n1}\rangle)$
	2D	2	$\frac{1}{2}$	$1/\sqrt{15}(2\sqrt{2}\cdot d_2\bar{d}_2 d_{n2}\rangle - \sqrt{2}\cdot d_2\bar{d}_1 d_{n1}\rangle + \sqrt{2}\cdot d_2\bar{d}_1 d_{n1}\rangle + \sqrt{3}\cdot d_1\bar{d}_1 d_0\rangle)$
	2D	2	$\frac{1}{2}$	$1/\sqrt{70}(- d_2\bar{d}_2 d_{n2}\rangle - 5\cdot d_2\bar{d}_1 d_{n1}\rangle + 3\cdot d_2\bar{d}_1 d_{n1}\rangle + 5\cdot d_2\bar{d}_0 d_0\rangle + 2\cdot d_2\bar{d}_1 d_{n1}\rangle + \sqrt{6}\cdot d_1\bar{d}_1 d_0\rangle)$
	2F	3	$\frac{1}{2}$	$1/2\sqrt{3}(\sqrt{6}\cdot d_2\bar{d}_2 d_{n1}\rangle - d_2\bar{d}_1 d_0\rangle - d_2\bar{d}_1 d_0\rangle + 2\cdot d_2\bar{d}_1 d_0\rangle)$
	4F	3	$\frac{3}{2}$	$ d_2\bar{d}_1 d_0\rangle$
	2G	4	$\frac{1}{2}$	$1/\sqrt{5}(\sqrt{2}\cdot d_2\bar{d}_2 d_0\rangle + \sqrt{3}\cdot d_2\bar{d}_1 d_1\rangle)$
	2H	5	$\frac{1}{2}$	$ d_2\bar{d}_2 d_1\rangle$

from the above single-particle subshells, with n_j electrons in subshell j (angular momentum u_j) such that $N = \sum_j n_j$. Using the decomposition in step 1, simultaneously diagonalize the pairwise commuting operators (5) acting on $\mathcal{C}^{n_1, \dots, n_k}$. (The parity operator \hat{R} is constant on $\mathcal{C}^{n_1, \dots, n_k}$ anyway and needs no further consideration.) In more detail, the isometry (9) and the decomposition (10) imply

$$\mathcal{C}^{n_1, \dots, n_k} \cong \bigoplus_{I=(i_1, \dots, i_k)} V_I, \quad V_I := \bigotimes_j V_{u_j, n_j, i_j}. \quad (11)$$

By construction, each V_I is uniquely characterized by its eigenvalues with respect to the LS operators L_j^2 and S_j^2 acting on the j th tensor factor. Since

$$L = \sum_j L_j, \quad S = \sum_j S_j,$$

all operators

$$L^2, S^2, L_{z_j}, S_{z_j}, \hat{R}, L_j^2, S_j^2 \quad j = 1, \dots, k$$

commute pairwise and it follows that each V_I is an invariant subspace of the operators (5). Thus, the diagonalization can be performed on each V_I independently. An explicit solution for the diagonalization in case of $k=2$ is well known in terms of the Clebsch–Gordan coefficients, which can be iteratively extended to higher k . We obtain

$$V_I = \bigoplus_{\substack{\ell s m_\ell m_s \\ |m_\ell| \leq \ell, |m_s| \leq s}} V_{I, \ell s m_\ell m_s} \quad (12)$$

such that for all $\varphi \in V_{I, \ell s m_\ell m_s}$,

$$L^2 \varphi = \ell(\ell + 1) \varphi, \quad L_z \varphi = m_\ell \varphi$$

$$S^2 \varphi = s(s + 1) \varphi, \quad S_z \varphi = m_s \varphi.$$

Note that $V_{I, \ell s m_\ell m_s}$ may be zero for some ℓ, s, m_ℓ, m_s .

Assembling Eqs. (11) and (12), we obtain

$$\mathcal{C}^{n_1, \dots, n_k} \simeq \bigoplus_{\ell s m_\ell m_s} V_{\ell s m_\ell m_s},$$

$$V_{\ell s m_\ell m_s} := \bigoplus_I V_{I, \ell s m_\ell m_s}.$$

That is, we have decomposed the configurations into the simultaneous eigenspaces of the angular momentum and spin operators (5)

C. Restriction to fixed m_ℓ and m_s

From general results about the angular momentum and spin algebra, it is well known that within an irreducible L^2 - S^2 -eigenspace, the ladder operators $L_\pm = L_x \pm iL_y$ and $S_\pm = S_x \pm iS_y$ traverse the L_z and S_z eigenstates, respectively. Additionally, the ladder operators commute with the Hamiltonian H in Eq. (3) as well as with the CI Hamiltonian. Thus, in terms of eigenvalue determination, it suffices to restrict to LS eigenstates with fixed m_ℓ and m_s . We adopt the convention in Ref. 16 and set $m_\ell \equiv 0$, $m_s \equiv s$ in the sequel.

D. Reduced density matrices

In this subsection, we will incorporate reduced density matrices (RDMs) (see, e.g., Refs. 4, 7, and 21) into the algorithmic framework to gain computational speedups and memory storage savings. In fact, we use RDMs of wave function pairs.

For any pair of states ψ and χ in the N -body Hilbert space (1), the matrix element of the Hamiltonian (3) can be rewritten as

$$\langle \chi | H \psi \rangle = \text{tr}_{\mathcal{H}} [h_0 \gamma_{|\psi\rangle\langle\chi|}] + \text{tr}_{\mathcal{H}} [v_{ee} \Gamma_{|\psi\rangle\langle\chi|}], \quad (13)$$

where $\gamma_{|\psi\rangle\langle\chi|}$ and $\Gamma_{|\psi\rangle\langle\chi|}$ are the one-body and two-body reduced density matrices of the N -body matrix $|\psi\rangle\langle\chi|$, respectively. Here, h_0 is the single-particle (hydrogen-like) Hamiltonian and v_{ee} is the interelectronic Coulomb potential,

$$h_0 = -\frac{1}{2} \Delta_{\mathbf{x}} - \frac{Z}{|\mathbf{x}|}, \quad v_{ee} = \frac{1}{|\mathbf{x} - \mathbf{y}|}. \quad (14)$$

Since these operators are independent of spin, we may effectively “trace out” the spin. With the standard notation

$$(ab|cd) := \int_{\mathbb{R}^6} \overline{a(\mathbf{x}_1)} b(\mathbf{x}_1) \frac{1}{|\mathbf{x}_1 - \mathbf{x}_2|} \overline{c(\mathbf{x}_2)} d(\mathbf{x}_2) d\mathbf{x}_1 d\mathbf{x}_2, \quad (15)$$

we obtain

$$\langle \chi | H | \psi \rangle = \text{tr}[\hat{h}_0 \hat{\gamma}_{|\psi\rangle\langle\chi|}] + \text{tr}[\hat{v}_{ee} \hat{\Gamma}_{|\psi\rangle\langle\chi|}], \quad (16)$$

with

$$(\hat{h}_0)_{i,j} := \langle i | h_0 | j \rangle, \quad (17)$$

$$(\hat{\gamma}_{|\psi\rangle\langle\chi|})_{i,j} := \sum_{\alpha} \langle i\alpha | \gamma_{|\psi\rangle\langle\chi|} | j\alpha \rangle, \quad (18)$$

$$(\hat{v}_{ee})_{ij,kl} := (ij|kl), \quad (19)$$

$$(\hat{\Gamma}_{|\psi\rangle\langle\chi|})_{k\ell,ij} := \sum_{\substack{\alpha, \beta \\ i\alpha < k\beta}} \langle j\alpha, \ell\beta | \Gamma_{|\psi\rangle\langle\chi|} | i\alpha, k\beta \rangle. \quad (20)$$

Here, i, j, k, ℓ denote spatial orbitals and $\alpha, \beta, \gamma, \delta$ are associated spin parts. The inequality constraint in the last sum refers to lexicographical ordering of spin orbitals.

By choosing the spatial orbitals real-valued, it follows that $(ij|k\ell) = (ji|k\ell)$ and $(ij|k\ell) = (ij|\ell k)$ for all i, j, k, ℓ . Thus, together with $(ij|k\ell) = (k\ell|ij)$, it suffices to calculate $(ij|k\ell)$ for $i \leq j$, $k \leq \ell$, and $(i, j) \leq (k, \ell)$ (in lexicographical order) only.

For our purposes, the following two features of the above RDM formalism are crucial. First, it avoids having to set up the full N -particle operators H_0 and V_{ee} , allowing one to work instead with the one-particle and two-particle operators h_0 and v_{ee} ; this leads to significant storage savings (see Sec. VI D). Second, the map from ψ and χ to $\hat{\Gamma}_{|\psi\rangle\langle\chi|}$ is an algebraic coefficient mapping which only depends on the symmetry types of the orbitals (i.e., s, p, d, \dots) and neither the radial wave functions nor the dilation parameters $Z_{n\ell}$. So the $\hat{\Gamma}_{|\psi\rangle\langle\chi|}$ can be precomputed for each angular momentum and spin symmetry eigenspace, without any reference to the Hamiltonian. The dilation parameters only enter the stage via the Coulomb integrals in \hat{v}_{ee} .

IV. HANDLING SLATER ORBITALS (STOS)

A. Orthonormalization

In this subsection, we formalize the orthonormalization calculations for STOs employed in Eq. 31 of Ref. 16. There, only $1s$, $2s$, and $2p$ wave functions are considered, whereas here, we handle arbitrary subshells.

More concretely, the wave functions are given by

$$\psi_{n\ell m}(\mathbf{x}) = s_{n\ell} r^\ell Y_{\ell m}(\vartheta, \varphi) \left(\sum_{i=0}^{n-\ell-1} b_{n\ell, i} c_{n\ell, i} r^i \right) e^{-Z_n \ell n r}, \quad (21)$$

$$r = |\mathbf{x}|, \quad \ell = 0, \dots, n-1, \quad n = 1, 2, \dots,$$

with $b_{n\ell, i}$ being the i th coefficient of the associated Laguerre polynomial $p(r) = L_{n-\ell-1}^{2\ell+1}(2r/n)$,

$$b_{n\ell, i} := \binom{n+\ell}{2\ell+1+i} \frac{(-2/n)^i}{i!},$$

and to-be determined orthogonalization coefficients $c_{n\ell, i} \in \mathbb{R}$ ($i=0, \dots, n-\ell-1$) as well as orthonormalization constants $s_{n\ell} > 0$. Since the spherical harmonics $Y_{\ell m}$ are orthogo-

nal, we may fix the angular momentum quantum numbers ℓ, m . Now using $\int_0^\infty r^n e^{-\lambda r} dr = \frac{n!}{\lambda^{n+1}}$, orthogonality translates to

$$\begin{aligned} 0 &= \langle \psi_{n\ell m} | \psi_{k\ell m} \rangle \\ &= \int_0^\infty \int_0^{2\pi} \int_0^\pi \overline{\psi_{n\ell m}(\mathbf{x})} \psi_{k\ell m}(\mathbf{x}) r^2 \sin \vartheta d\vartheta d\varphi dr \\ &= \overline{s_{n\ell} s_{k\ell}} \sum_{i,j} b_{n\ell,i} \overline{b_{k\ell,j}} \overline{c_{n\ell,i}} c_{k\ell,j} \frac{(i+j+2\ell+2)!}{\left(\frac{Z_{n\ell}}{n} + \frac{Z_{k\ell}}{k}\right)^{i+j+2\ell+3}} \\ &= \overline{s_{n\ell} s_{k\ell}} \langle c_{n\ell} | B_{n\ell} H_{nk}^\ell B_{k\ell} c_{k\ell} \rangle \end{aligned} \quad (22)$$

for all $k = \ell + 1, \dots, n - 1$. Here we have extended the vectors $(c_{k\ell,i})_{i=0, \dots, k-\ell-1}$ by $c_{k\ell,i} = 0$ for $i \geq k - \ell$. The Hankel matrix H_{nk}^ℓ is defined by

$$H_{nk}^\ell := (a_{i+j}^\ell(\lambda))_{i,j} |_{\lambda = (Z_{n\ell}/n) + Z_{k\ell}/k}, \quad a_i^\ell(\lambda) := \frac{(i+2(\ell+1))!}{\lambda^{i+2\ell+3}}$$

and $B_{n\ell}$ is the diagonal matrix $\text{diag}(b_{n\ell,i})_i$. Summarizing Eq. (22), we obtain

$$c_{n\ell} \perp \text{span}(B_{n\ell} H_{nk}^\ell B_{k\ell} c_{k\ell})_{k=\ell+1, \dots, n-1}, \quad (23)$$

so $c_{n\ell}$ can be calculated iteratively for $n = \ell + 1, \ell + 2, \dots$ starting from the convention $c_{(\ell+1)\ell,0} = 1$.

Note that the a_i^ℓ are the moments of a nonnegative measure m on the positive real axis \mathbb{R}_+ . Namely, let $dm_{\lambda,\ell}(t) = t^{2(\ell+1)} e^{-\lambda t} dt$, then

$$a_i^\ell(\lambda) = \int_{\mathbb{R}_+} t^i dm_{\lambda,\ell}(t).$$

The Stieltjes moment problem²² states that this is equivalent to the quadratic form given by H_{nk}^ℓ being positive.

Once all $c_{n\ell}$ have been obtained, we may plug $k = n$ into Eq. (22) to calculate the normalization factors $s_{n\ell}$ from

$$1 \stackrel{!}{=} \langle \psi_{n\ell m} | \psi_{n\ell m} \rangle = |s_{n\ell}|^2 \langle c_{n\ell} | B_{n\ell} H_{nn}^\ell B_{n\ell} c_{n\ell} \rangle. \quad (24)$$

B. One-body integrals

The one-body matrix elements

$$\langle \psi_{n\ell m} | \psi_{n'\ell' m'} \rangle := \langle \psi_{n\ell m} | h_0 | \psi_{n'\ell' m'} \rangle \quad (25)$$

$$= \int_{\mathbb{R}^3} \left(\frac{1}{2} \nabla \overline{\psi_{n\ell m}} \cdot \nabla \psi_{n'\ell' m'} - \frac{Z}{|\mathbf{x}|} \overline{\psi_{n\ell m}} \psi_{n'\ell' m'} \right) d^3 \mathbf{x}$$

can be evaluated symbolically from Eq. (21) by a computer algebra system, via symbolic differentiation and exact integration in spherical polar coordinates.

C. Two-body integrals

1. Switching to real-valued, Cartesian coordinates

As mentioned in Sec. III D, we save computational costs by switching to real-valued spatial orbitals when calculating Coulomb integrals. Thus, for each fixed ℓ , we apply a unitary base change $U_\ell = (u_{\ell,mm'})_{mm'}$ to the spherical harmonics $Y_{\ell m}$ of degree ℓ to obtain real-valued polynomials in Cartesian coordinates,

$$Z_{\ell m}(\mathbf{x}) := r^\ell \sum_{m'=\ell, \ell-1, \dots, -\ell} u_{\ell,mm'} Y_{\ell m'} \stackrel{!}{=} \sum_{p_1+p_2+p_3=\ell} c_{\ell m, \mathbf{p}} \cdot \mathbf{x}^{\mathbf{p}},$$

where $c_{\ell m, \mathbf{p}} \in \mathbb{R}$ and $\mathbf{x}^{\mathbf{q}} := \prod_{i=1}^3 x_i^{q_i}$. Plugging this into Eq. (21) results in real-valued Slater-type orbitals given by

$$\psi_{n\ell m}(\mathbf{x}) = s_{n\ell} Z_{\ell m}(\mathbf{x}) \left(\sum_{i=0}^{n-\ell-1} d_{n\ell,i} r^i \right) e^{-Z_{n\ell} r}, \quad (26)$$

where we have set $d_{n\ell,i} := b_{n\ell,i} c_{n\ell,i}$ to shorten notation.

Concretely, for $\ell = 1$, we adapt Ref. 16 and choose (in this order)

$$(Z_{1m}(\mathbf{x}))_m = (pz, px, py) := \frac{1}{2} \sqrt{\frac{3}{\pi}} (x_3, x_1, x_2).$$

For $\ell = 2$,

$$\begin{aligned} (Z_{2m}(\mathbf{x}))_m = (d0, dz, dm, dx, dy) &:= \frac{1}{4} \sqrt{\frac{15}{\pi}} \\ &\times \left(\frac{2x_3^2 - x_1^2 - x_2^2}{\sqrt{3}}, 2x_1 x_2, x_1^2 - x_2^2, 2x_2 x_3, 2x_1 x_3 \right), \end{aligned}$$

or, figuratively, $dx \sim 2yz$, $dy \sim 2xz$, $dz \sim 2xy$, $d0 \sim (3z^2 - r^2)/\sqrt{3}$, and $dm \sim x^2 - y^2$. The corresponding unitary U_ℓ read

$$U_1 = \frac{1}{\sqrt{2}} \begin{pmatrix} 0 & \sqrt{2} & 0 \\ -1 & 0 & 1 \\ i & 0 & i \end{pmatrix}$$

and

$$U_2 = \frac{1}{\sqrt{2}} \begin{pmatrix} 0 & 0 & \sqrt{2} & 0 & 0 \\ -i & 0 & 0 & 0 & i \\ 1 & 0 & 0 & 0 & 1 \\ 0 & i & 0 & i & 0 \\ 0 & -1 & 0 & 1 & 0 \end{pmatrix}$$

when arranging the spherical harmonics $Y_{\ell m}$ with decreasing quantum number m .

2. Transformation to Fourier space

We adapt the idea in Ref. 16 to calculate Coulomb integrals between pairs of spatial orbitals by applying Fourier transformation. We use the normalization-factor-free convention

$$(\mathcal{F}f)(\mathbf{k}) := \int_{\mathbb{R}^n} f(\mathbf{x}) e^{-i\mathbf{k} \cdot \mathbf{x}} d\mathbf{x}.$$

Given one-electron orbitals $\varphi_1, \varphi_2, \dots$ with φ_i and $\mathcal{F}\varphi_i \in L^2(\mathbb{R}^3) \cap L^\infty(\mathbb{R}^3)$, let $f(\mathbf{x}) := \varphi_i(\mathbf{x}) \varphi_j(\mathbf{x})$ and $g(\mathbf{x}) := \varphi_k(\mathbf{x}) \varphi_\ell(\mathbf{x})$. Then (see, e.g., Ref. 16)

$$\langle \varphi_i \varphi_j | \varphi_k \varphi_\ell \rangle = \frac{1}{2\pi^2} \int_{\mathbb{R}^3} \frac{1}{|\mathbf{k}|^2} \overline{(\mathcal{F}f)(\mathbf{k})} (\mathcal{F}g)(\mathbf{k}) d^3 \mathbf{k}.$$

Since we have switched to real-valued Cartesian orbitals in Sec. IV C 1, $f(\mathbf{x}) = \varphi_i(\mathbf{x}) \overline{\varphi_j(\mathbf{x})}$ can be expanded as

$$f(\mathbf{x}) = \sum_{\nu=0}^{\nu_{\max}} r^{\nu} \left(\sum_{q_1, q_2, q_3=0}^{q_{\max}} c_{\nu, q} \cdot \mathbf{x}^q \right) e^{-\lambda r}, \quad r = |\mathbf{x}| \quad (27)$$

with constants $c_{\nu, q}$ and $\lambda > 0$. Directly from the definition of the Fourier transformation, it follows that

$$(\mathcal{F}f)(\mathbf{k}) = \sum_{\nu, q} c_{\nu, q} (-1)^{\nu} \frac{\partial^{\nu}}{\partial \lambda^{\nu}} i^{q_1+q_2+q_3} \frac{\partial^q}{\partial \mathbf{k}^q} (\mathcal{F}e^{-\lambda r})(\mathbf{k}), \quad (28)$$

where we have used the notation

$$\frac{\partial^q}{\partial \mathbf{k}^q} := \prod_{i=1}^3 \frac{\partial^{q_i}}{\partial k_i^{q_i}} \quad \text{for each } \mathbf{q} \in \mathbb{N}_0^3.$$

It is well known that

$$(\mathcal{F}e^{-\lambda r})(\mathbf{k}) = \frac{8\lambda\pi}{(\lambda^2 + k^2)^2}, \quad k = |\mathbf{k}|.$$

Thus, precomputing the following integral over polar coordinates:

$$\begin{aligned} I_{q, q'}(\lambda, \lambda') &:= (-i)^{q_1+q_2+q_3; q'_1+q'_2+q'_3} \frac{1}{2\pi^2} \\ &\times \int_0^{\infty} \int_0^{\pi} \int_0^{2\pi} \left(\frac{\partial^q}{\partial \mathbf{k}^q} \frac{8\lambda\pi}{(\lambda^2 + k^2)^2} \right) \\ &\times \left(\frac{\partial^{q'}}{\partial \mathbf{k}'^q} \frac{8\lambda'\pi}{(\lambda'^2 + k'^2)^2} \right) \sin \vartheta d\varphi d\vartheta dk \end{aligned}$$

we obtain for the spinless Coulomb integrals (19) with orbitals (21)

$$\begin{aligned} (\hat{v}_{ee})_{ij,kl} &= (\varphi_i \varphi_j | \varphi_k \varphi_l) \\ &= \sum_{\nu, \nu'} \sum_{q, q'} \overline{c_{\nu, q}} c_{\nu', q'} \cdot (-1)^{\nu+\nu'} \frac{\partial^{\nu}}{\partial \lambda^{\nu}} \frac{\partial^{\nu'}}{\partial \lambda'^{\nu'}} I_{q, q'}(\lambda, \lambda'), \end{aligned} \quad (29)$$

with $c_{\nu, q}$ and λ as in Eq. (27) and $c_{\nu', q'}$ and λ' as the analogous constants for $\varphi_k(x)\varphi_l(x)$.

3. Application to dilated Slater-type orbitals

Taking pairwise products of the wave functions (26) involves the convolution of coefficients

$$\begin{aligned} f(\mathbf{x}) &:= \psi_{n\ell m}(\mathbf{x}) \overline{\psi_{n'\ell' m'}(\mathbf{x})} = s_{n\ell} s_{n'\ell'} Z_{\ell m}(\mathbf{x}) Z_{\ell' m'}(\mathbf{x}) \\ &\times \left(\sum_i (d_{n\ell} * d_{n'\ell'})_i r^i \right) e^{-(Z_{n\ell}/n + Z_{n'\ell'}/n')r} \end{aligned}$$

with the discrete convolution

$$(d_{n\ell} * d_{n'\ell'})_i = \sum_k d_{n\ell, k} d_{n'\ell', i-k}.$$

Similar reasoning applies to the product $Z_{\ell m} Z_{\ell' m'}$,

$$Z_{\ell m}(\mathbf{x}) Z_{\ell' m'}(\mathbf{x}) = \sum_{|p|=|\ell+\ell'|} (c_{\ell m} * c_{\ell' m'})_p \cdot \mathbf{x}^p.$$

Let

$$g(\mathbf{x}) := \overline{\psi_{\tilde{n}\tilde{\ell}\tilde{m}}(\mathbf{x})} \psi_{\tilde{n}'\tilde{\ell}'\tilde{m}'}(\mathbf{x})$$

be another pairwise product of wave functions. Then the Coulomb integral of these pairs equals

$$\begin{aligned} (\psi_{n\ell m} \psi_{n'\ell' m'} | \psi_{\tilde{n}\tilde{\ell}\tilde{m}} \psi_{\tilde{n}'\tilde{\ell}'\tilde{m}'}) &= \int \int_{\mathbb{R}^3} \frac{\overline{f(\mathbf{x})} g(\mathbf{y})}{|\mathbf{x}-\mathbf{y}|} d^3\mathbf{x} d^3\mathbf{y} \stackrel{(29)}{=} s_{n\ell} s_{n'\ell'} s_{\tilde{n}\tilde{\ell}} s_{\tilde{n}'\tilde{\ell}'} \sum_i (d_{n\ell} * d_{n'\ell'})_i \sum_j (d_{\tilde{n}\tilde{\ell}} * d_{\tilde{n}'\tilde{\ell}'})_j \\ &\times \sum_{|p|=|\ell+\ell'|} (c_{\ell m} * c_{\ell' m'})_p \sum_{|q|=|\tilde{\ell}+\tilde{\ell}'|} (c_{\tilde{\ell} \tilde{m}} * c_{\tilde{\ell}' \tilde{m}'})_q \\ &\times (-1)^{i+j} \frac{\partial^i}{\partial \lambda^i} \frac{\partial^j}{\partial \mu^j} I_{p, q}(\lambda, \mu) \Big|_{\lambda=Z_{n\ell}/n+Z_{n'\ell'}/n', \mu=Z_{\tilde{n}\tilde{\ell}}/\tilde{n}+Z_{\tilde{n}'\tilde{\ell}'}/\tilde{n}'}. \end{aligned} \quad (30)$$

V. COMPUTING THE CI LEVELS AND STATES

Our overall algorithm for the CI method in Sec. II C consists of a symbolic part (symmetry reduction and reduction to two-body space) and a numerical part (Hamiltonian matrix diagonalization and orbital exponent optimization).

A. Symbolic precomputation

The following precomputational steps will allow us to calculate the matrix representation of the Hamiltonian quickly, given plug-in values for the dilation parameters $Z_{n\ell}$:

- (1) Compute the simultaneous eigenspaces of the operators (5), via the algorithm described in Sec. III B.

- (2) For any simultaneous eigenspace of the operators (5), choose an orthonormal basis (ψ_1, \dots, ψ_r) and calculate the one-particle and two-particle reduced density matrices $\gamma_{|\psi_i\rangle\langle\psi_j|}$ and $\Gamma_{|\psi_i\rangle\langle\psi_j|}$, respectively, of the N -particle states $|\psi_i\rangle\langle\psi_j|$ for all $i, j=1, \dots, r$. Subsequently, trace out the spin part as defined in Eqs. (20) and (18) to obtain $\hat{\gamma}_{|\psi_i\rangle\langle\psi_j|}$ and $\hat{\Gamma}_{|\psi_i\rangle\langle\psi_j|}$.
- (3) For the Slater orbitals (21), calculate symbolic versions of the orthonormalization constants $c_{n\ell}$ and $s_{n\ell}$ in Sec. IV A via Eqs. (23) and (24), respectively. Note that these constants still depend on the dilation parameters $Z_{n\ell}$, which will be plugged in at the numerical optimization step below.

- (4) Calculate symbolic matrix representations (17) and (19) of the single-particle and electron-interaction Hamiltonians h_0 and v_{ee} using, a computer algebra system, and Eq. (25) for h_0 and Eq. (30) for v_{ee} . These matrices still depend on the orthonormalization constants $s_{n\ell}$ and $c_{n\ell,i}$ from step 2 and on the dilation parameters $Z_{n\ell}$.

B. Numerical diagonalization and energy minimization

For any given set of orbital exponents $Z_{n\ell}$, we can now calculate and diagonalize the matrix representation of the Hamiltonian projected onto any LS eigenspace by using the reduced density matrix formalism in Sec. III D. In mathematical terms,

- (1) For a current numerical value of the orbital exponents $Z_{1,0}, Z_{2,0}, Z_{2,1}, \dots$, evaluate the symbolic orthonormalization constants $s_{n\ell}$ and $c_{n\ell,i}$ and the symbolic matrix elements of \hat{h}_0 and \hat{v}_{ee} .
- (2) Equation (16) yields the matrix elements of the Hamiltonian on an LS eigenspace with orthonormal basis (ψ_1, \dots, ψ_r) , namely,

$$\langle \psi_i | H | \psi_j \rangle = \text{tr}(\hat{h}_0 \hat{\gamma}_{|\psi_j\rangle\langle\psi_i|}) + \text{tr}(\hat{v}_{ee} \hat{\Gamma}_{|\psi_j\rangle\langle\psi_i|}).$$

(Note that it would be theoretically possible but computationally inefficient to carry out this step symbolically.)

- (3) Obtain the ground state energy $E = \lambda_{\min}(\langle \psi_i | H | \psi_j \rangle_{i,j=1,\dots,r})$.
- (4) Iteratively repeat these steps for different values of the orbital exponents within a suitable optimization routine to minimize the ground state energy numerically. (We used a gradient-free simplex search method.)

VI. COST ANALYSIS

In what follows, we review the computational speedup of the central algorithmic steps as compared to operating directly on the full N -particle Hilbert space $\wedge^N \mathcal{H}$.

A. Configurations

In this paragraph, we quantify the savings by the configuration calculus introduced in Sec. III A. To shorten notation, set $g_j := \dim V_{u_j}$ and assume that the total particle number N is fixed. Thus, the dimension of the full N -particle Hilbert space equals $\binom{\sum g_j}{N}$. Consider configurations C^{n_1, \dots, n_k} with $\sum n_j = N$. They partition the Hilbert space and accordingly,

$$\begin{aligned} \sum_{\substack{n_1, \dots, n_k \\ \sum n_j = N}} \dim(C^{n_1, \dots, n_k}) &= \sum_{\substack{n_1, \dots, n_k \\ \sum n_j = N}} \prod_j \binom{g_j}{n_j} \\ &= \binom{\sum g_j}{N} = \dim(\wedge^N \mathcal{H}) \end{aligned}$$

as expected. Now, assume we are given an algorithm of order $\mathcal{O}(\dim^p)$, such as, e.g., LS diagonalization with $p=3$. Run-

ning this algorithm either applied to all configurations separately or to the full N -particle Hilbert space incurs computational costs of order

$$\sum_{\substack{n_1, \dots, n_k \\ \sum n_j = N}} \dim(C^{n_1, \dots, n_k})^p \quad \text{as compared to} \quad \dim(\wedge^N \mathcal{H})^p. \quad (31)$$

In what follows, we derive an estimate of the quotient of these two terms. The Stirling approximation of factorials and a logarithmic series expansion leads to

$$\binom{g}{n} \approx 2^{1/2+g} (\pi g)^{-1/2} e^{-(g-2n)^2/2g}.$$

Plugging this into the left hand side of Eq. (31) yields

$$\begin{aligned} \sum_{\substack{n_1, \dots, n_k \\ \sum n_j = N}} \prod_j \binom{g_j}{n_j}^p &\approx \int \cdots \int_{-\infty}^{\infty} \delta(N - \sum n_j) \\ &\prod_j 2^{p((1/2)+g_j)} (\pi g_j)^{-p/2} e^{-p(g_j - 2n_j)^2/2g_j} \mathrm{d}n_1 \cdots \mathrm{d}n_k. \end{aligned}$$

The Fourier transform of these integrals is the pointwise product of the individual Fourier transforms. One obtains

$$\begin{aligned} \int_{-\infty}^{\infty} 2^{p(1/2+g)} (\pi g)^{-p/2} e^{-p(g-2n)^2/2g} e^{-int} \mathrm{d}n \\ = (2/\pi)^{1/2(p-1)} p^{-1/2} 2^{pg} g^{1/2(1-p)} e^{-gt(4ip+t)/(8p)} \end{aligned}$$

for each individual transform. Now, the inverse Fourier transform of the pointwise products gives the desired approximation of the left hand side of Eq. (31), namely,

$$\begin{aligned} (2/\pi)^{1/2(1-k+kp)} p^{1/2(1-k)} (g_{\text{prod}})^{1/2(1-p)} \\ \times 2^{pg_{\text{sum}}} (g_{\text{sum}})^{-1/2} e^{-p(g_{\text{sum}} - 2N)^2/2g_{\text{sum}}}, \end{aligned} \quad (32)$$

where we have set $g_{\text{sum}} := \sum_j g_j$ and $g_{\text{prod}} := \prod_j g_j$ to shorten notation. Finally, dividing the (Stirling approximated) right hand side of Eq. (31) by Eq. (32) yields the sought-after quotient

$$\left(\frac{\pi}{2}\right)^{1/2(k-1)(p-1)} p^{1/2(k-1)} \left(\frac{g_{\text{prod}}}{g_{\text{sum}}}\right)^{1/2(p-1)}.$$

Note that this factor is independent of the particle number N . It equals 1 for $p=1$, as expected.

As concrete example, consider chromium with three active subshells $3p, 3d, 4s$, i.e., all subshells up to $3s$ are completely filled. Thus, in terms of the computation parameters, we have $(g_1, g_2, g_3) \equiv (\dim V_p, \dim V_d, \dim V_s) = (6, 10, 2)$, $N_{\text{eff}} = 12$ (electron number in active orbitals), and algorithmic order $p=3$, say. Then, the approximated quotient equals $5\pi^2 \doteq 49.348$, which is close to the exact number $50\,774\,322\,144/938\,076\,521 \doteq 54.1$.

B. LS diagonalization for sparse vectors

In this paragraph, we show that the cost of the decomposition (12) essentially scales linearly in the problem size $\dim(V_j)$, assuming a sparse structure of the associated coefficient vectors.

First, consider two irreducible angular momentum eigenspaces V_1 and V_2 with quantum numbers ℓ_j and dimensions $(2\ell_j+1)$ ($j=1,2$, without loss of generality $\ell_1 \geq \ell_2$). Then the Clebsch–Gordan method partitions $V_1 \oplus V_2$ into total angular momentum eigenstates, i.e.,

$$V_1 \otimes V_2 = \bigoplus_{\ell=|\ell_1-\ell_2|}^{\ell_1+\ell_2} V_{12,\ell}, \quad \dim(V_{12,\ell}) = 2\ell + 1.$$

Each $V_{12,\ell}$ requires the computation of exactly

$$\text{num}_{\text{CG}}(V_{12,\ell}) = (\ell_1 + \ell_2 + 1)(2\ell + 1) - (\ell_1 - \ell_2)^2 - \ell(\ell + 1) \quad (33)$$

Clebsch–Gordan coefficients and Kronecker products $\varphi_1 \otimes \varphi_2$ ($\varphi_j \in V_j$). Due to the mentioned sparse structure, we assume $\mathcal{O}(1)$ cost for each of these Kronecker products. Summing up Eq. (33) for all ℓ yields

$$\begin{aligned} & \sum_{\ell=|\ell_1-\ell_2|}^{\ell_1+\ell_2} \text{num}_{\text{CG}}(V_{12,\ell}) \\ &= (2\ell_2 + 1) \left[(2\ell_1 + 1)(2\ell_2 + 1) - \frac{1}{3}((2\ell_2 + 1)^2 - 1) \right] \\ &\leq (2\ell_2 + 1)\dim(V_1 \otimes V_2). \end{aligned} \quad (34)$$

Now consider irreducible angular momentum eigenspaces V_j , $j=1, \dots, k$, with respective quantum numbers ℓ_j . The computational cost of the iterated Clebsch–Gordan method will be dominated by the calculation of the total angular momentum eigenspaces of

$$\left(\bigoplus_i V_{1, \dots, k-1; \tilde{\ell}_i} \right) \bigoplus V_k, \quad \dim(V_{1, \dots, k-1; \tilde{\ell}_i}) = 2\tilde{\ell}_i + 1,$$

where each $V_{1, \dots, k-1; \tilde{\ell}_i}$ is an irreducible angular momentum eigenspace in $\bigotimes_{j=1}^{k-1} V_j$ such that $\sum_i (2\tilde{\ell}_i + 1) = \dim(V_1 \otimes \dots \otimes V_{k-1})$. According to Eq. (34), this requires not more than $(2\ell_k + 1) \cdot \dim(V_1 \otimes \dots \otimes V_k)$ Clebsch–Gordan coefficients and associated Kronecker products. Thus, in case of all V_j being of uniformly bounded dimension, i.e., $\ell_1, \dots, \ell_k \leq \ell_{\max}$, the cost is of order

$$\text{cost}_{\text{CG}}(V_1, \dots, V_k) = \mathcal{O}(\dim(V_1 \otimes \dots \otimes V_k)). \quad (35)$$

So indeed, the cost is (almost) of the order of the problem size.

The analysis for spin states is exactly the same and the angular momentum and spin operators can be treated independently. Thus, the result (35) remains valid when considering both angular momentum and spin.

C. Diagonalization of the Hamiltonian

We now consider the exact reduction steps introduced in Secs. II A and III C: the Hamiltonian can be diagonalized within each LS eigenstate separately and only states with

quantum numbers $m_\ell \equiv 0$, $m_s \equiv s$ need to be taken into account. (Partitioning into configurations is advantageous for the LS diagonalization only, since the Hamiltonian mixes configurations.) The latter saves a factor of $(2\ell+1) \cdot (2s+1)$ states with each L^2 - S^2 eigenspace. The former, in the examples in Sec. VII, reduces the number of states by a factor of 10^2 – 10^3 .

We illustrate the huge cost reduction by the example of the chromium 7S states with configurations $[\text{Ar}]3d^i4s4p^k4d^\ell$ such that $j+k+\ell=5$ (see Sec. VII). The dimension of the full CI state space equals $\binom{26}{5}=65\,780$ (since five valence electrons have to be allocated to $10+6+10$ possible orbitals). By contrast, restricting to a typical symmetry subspace of interest, such as 7S (i.e., $L^2=0$ and $S^2=3(3+1)$), reduces the dimension to 98 and taking S_z maximal and $L_z=0$ reduces it further to 14.

D. Storing RDMs instead of N -particle wave functions

Even though the number of required wave functions has been reduced, each individual N -electron wave function on a K -orbital space still requires, *a priori*, $\binom{K}{N}$ entries.

First—as illustrated in Sec. III D—this cost can be reduced since the components of the Hamiltonian matrix on a given N -particle subspace only requires knowledge of the two-particle density matrices of any pair of N -particle basis functions. These RDMs have $\binom{K}{2}^2 = \mathcal{O}(K^4)$ entries, namely, $(\Gamma_{|\psi\rangle\langle\chi|})_{ij,kl}$ with $1 \leq i < j \leq K$ and $1 \leq k < l \leq K$.

Second, applying the spinless density matrix defined in Eq. (20) reduces the number K of single-particle orbitals by one half.

Third, we note that the density matrix typically exhibits a sparse structure, so we actually need far fewer entries. This is related to prior LS diagonalization on the N -particle Hilbert space. More precisely, the two-particle RDM of an N -particle L^2 - S^2 - L_z - S_z eigenstate must commute with these symmetry operators on the two-particle space. Reconsider, for instance, the 7S states of chromium with configuration $[\text{Ar}]3d^i4s4p^k4d^\ell$, where $j+k+\ell=5$. A general spinless RDM with orbitals up to $4d$ has $\binom{23+1}{2}^2=76\,176$ entries. By contrast, the $14^2=196$ RDMs of the 14 7S states with S_z maximal and $L_z=0$ turn out to have, on average, only 94.3 nonzero entries, the maximum number of nonzero entries which occurs being 648.

VII. ANOMALOUS FILLING OF 4s AND 3d ORBITALS IN TRANSITION METAL ATOMS

We have applied the algorithmic framework reported above to the calculation of ground and excited states and levels in 3d transition metal atoms. These continue to offer substantial computational challenges, due to the irregular filling of 4s versus 3d orbitals, strong correlations, and non-negligible relativistic effects.

Previous computations have led to different results, depending on the level of theory used. Limitations of single-determinant Hartree–Fock theory for these atoms are discussed in Ref. 11. Multideterminant Hartree–Fock (HF) energies for the experimental ground state configurations (but not for competing configurations) are given in Ref. 23

TABLE II. Ground state symmetries and energies from K to Zn predicted by minimal asymptotics-based CI (this paper) with active space $[\text{Ar}]3d^j4s^k$ and compared to experimental data (Ref. 26). Boldface denotes deviation from experiment. The dimension of the joint eigenspace of the symmetry operators (5) which contains the unique ground state with $L_z=0$ and S_z maximal is denoted by dim. Also shown are multi-determinant Hartree–Fock energies for the experimental ground state symmetries (Ref. 25) (for Ti and Cr, see also Refs. 24 and 27).

Atom	Symmetry			Energy (a.u.)		
	CI	exp	dim (subspace)	CI	Exp	MDHF
K	2S	2S	1	-596.7993	-601.9337	-599.164 78
Ca	1S	1S	2	-674.2442	-680.1920	-676.758 18
Sc	2D	2D	4	-756.8908	-763.8673	-759.735 71
Ti	3F	3F	5	-845.1599	-853.3503	-848.405 99
V	4F	4F	4	-939.1657	-948.8394	-942.884 33
Cr	5D	7S	3	-1039.0409	-1050.4914	-1043.3563
Mn	6S	6S	1	-1144.9715	-1158.2670	-1149.8662
Fe	5D	5D	1	-1256.7813	-1271.6930	-1262.4436
Co	4F	4F	2	-1374.8903	-1393.3526	-1381.4145
Ni	3F	3F	1	-1499.3759	-1520.6907	-1506.8709
Cu	2D	2S	1	-1630.3692	-1655.1317	-1638.9637
Zn	1S	1S	1	-1768.0729	...	-1777.8481

(with the exception of Cr), Ref. 24 (only for atoms with anomalous filling such as Cr), and Ref. 25. The interconfigurational ordering of $4s^13d^n$ versus $4s^23d^{n-1}$ is discussed in Ref. 12 for relativistic HF and in Refs. 13 and 14 for DFT. Among the transition metal series Sc, Ti, V, Cr, Mn, Fe, Co, Ni, Cu, relativistic HF rendered $4s^1$ stable for Cr, Mn, Fe, Ni, and Cu, even though experimentally only Cr and Cu have a $4s^1$ ground state. [In fact, for Ni, the experimental classification as $4s^2$ should be viewed with some caution. A look at the actual data²⁶ shows that for Ni, relativistic J splittings are of the same order as the interconfigurational gap, and while the experimental ground state is a particular J state of the $4s^2$ (3F) configuration, $4s^1$ (3D) would become stable if one averages over J according to multiplicity.] DFT does not fare better, regardless of the type of exchange-correlation functional used: $4s^1$ is rendered stable by Becke 88 for Ti, V, Cr, Ni, and Cu,¹⁴ by the local density approximation and Perdew–Wang for V, Cr, Co, Ni, and Cu,^{13,14} and by B3LYP for V, Cr, Co, Ni, and Cu.¹⁴ The poor atomization energies of DFT functionals such as Becke 88 and B3LYP for transition metal dimers (those for Cr_2 even come out with the wrong sign) have been associated¹⁴ to poor interconfigurational energies of the atoms. It is then of interest to revisit the latter from alternative theoretical points of view.

Our results for the asymptotics-based CI model (A)–(C) in Sec. II C are as follows. First, we considered a minimal model for the third period elements K to Zn with configurations $[\text{Ar}]3d^j4s^k$, that is to say in the language of Sec. II C, we choose the cutoffs

$$(n, \ell)_{\min} = (3, 1) = 3p, \quad (n, \ell)_{\max} = (4, 0) = 4s.$$

It turns out that the ground states from Ca to Zn always put two electrons in the $4s$ subshell, i.e., have configuration $[\text{Ar}]3d^j4s^2$ (see Table II). Thus minimal asymptotics-based CI coincides with the empirical Madelung rule (which states

that the subshells are filled in the order of increasing $n+\ell$ and, for equal $n+\ell$, in the order of decreasing n). Experimentally, this means that the method fails for the two anomalous atoms Cr and Cu.

Next, to address this issue we enlarged the CI subspace for the series Ca, Sc, Ti, V, Cr by the higher subshells $4p$ and $4d$. That is to say we changed the cutoffs to

$$(n, \ell)_{\min} = (3, 1) = 3p, \quad (n, \ell)_{\max} = (4, 2) = 4d,$$

hence including all configurations $[\text{Ar}]4d^j4s^k4p^\ell4d^m$ and restricted to $k=1$ ($4s^1$) and $k=2$ ($4s^2$), respectively. In each case, we considered only the L and S values selected by Hund’s rules (i.e., we minimized first S and then L , taking into account one s and d subshell as in the minimal model above), computed the corresponding symmetry subspaces via the algorithm in Sec. III B, and determined the associated eigenstates and energy levels. The results are shown in Table III.

Despite the smallness of the radial basis set, the predicted ground state configurations and spin and angular momentum quantum numbers are in full agreement with the experimental data. Physically, interesting insights can be gained from the orbital exponents in Table III and from the coefficients of the different configurations contained in the ground state. First, for Ca, the $4s$ electron is more tightly bound than any d electrons, whereas for Sc, Ti, V, and Cr, this effect is reversed in both the $4s^1$ and the $4s^2$ configuration, with $4s$ outside of both $3d$ and $4d$. Second, considering, for instance, the $4s^1$ (7S) Cr ground state, the configurations and weight coefficients of the 14 contributing basis states spanning the 7S , $m_L=0$, and $m_S=3$ symmetry subspace of $3d^j4s^14p^\ell4d^m$ are as follows:

TABLE III. Asymptotics-based CI results with active space $[\text{Ar}]3d^i4s^14p^k4d^l$ and $[\text{Ar}]3d^i4s^24p^k4d^l$, respectively (this paper); boldface denotes the experimental ground state symmetry and italic denotes the lower of each pair of calculated energies, in exact agreement with the experimental data. Fourth column: Dimension of the symmetry subspace containing the ground state.

	Symmetry	Configuration	Dimension	E_{CI} (a.u.)	Z_{1s}	Z_{2s}	Z_{2p}	Z_{3s}	Z_{3p}	Z_{3d}	Z_{4s}	Z_{4p}	Z_{4d}
Ca	3D	$4s^1$	2	-674.1634	19.68	17.41	16.13	12.05	10.38	2.83	5.43	...	2.46
	1S	$4s^2$	1	-674.2442	19.68	17.41	16.13	12.10	10.38	...	5.03
Sc	4F	$4s^1$	3	-756.9381	20.68	18.42	17.15	12.99	11.30	8.26	5.35	...	6.24
	2D	$4s^2$	2	-756.9968	20.68	18.42	17.15	13.06	11.34	10.07	5.31	...	8.46
Ti	5F	$4s^1$	8	-845.3714	21.68	19.43	18.16	13.89	12.18	9.91	5.51	1.45	7.75
	3F	$4s^2$	3	-845.4210	21.68	19.43	18.16	13.98	12.23	11.30	5.52	...	9.67
V	6D	$4s^1$	17	-939.5952	22.68	20.44	19.17	14.78	13.04	11.20	5.61	1.88	8.93
	4F	$4s^2$	8	-939.6375	22.68	20.44	19.17	14.86	13.10	12.36	5.70	5.25	10.62
Cr	7S	$4s^1$	14	-1039.7864	23.68	21.44	20.18	15.64	13.89	12.37	5.67	9.51	10.00
	5D	$4s^2$	17	-1039.7852	23.68	21.44	20.18	15.74	13.95	13.36	5.87	0.93	11.49

$3d^54p^04d^0$	0.36
$3d^44p^04d^1$	0.63
$3d^34p^24d^0$	0.056
$3d^34p^04d^2$ (2D)	0.31 and 0.50
$3d^24p^24d^1$ (2D)	0.036 and 0.038
$3d^24p^04d^3$ (2D)	0.17 and 0.28
$3d^14p^24d^2$ (2D)	0.016 and 0.014
$3d^14p^04d^4$	0.096
$3d^04p^24d^3$	0.0036
$3d^04p^04d^5$	0.012

In particular, no configuration dominates and the highest weight configuration is not the naively expected $3d^5$ which one would enforce in both single-determinant HF and (L - S adapted) multi-determinant HF, but $3d^44d^1$ (weight 0.63), followed by $3d^34d^2$ (0.59), $3d^5$ (0.36), and $3d^24d^3$ (0.33). The highest-weight Cr 7S basis function in which one of the $3d$ electrons has migrated to a $4d$ orbital is

$$(|3d_23d_13d_03d_{n1}4s4d_{n2}\rangle - |3d_23d_13d_03d_{n2}4s4d_{n1}\rangle + |3d_23d_13d_{n1}3d_{n2}4s4d_0\rangle - |3d_23d_03d_{n1}3d_{n2}4s4d_1\rangle + |3d_13d_03d_{n1}3d_{n2}4s4d_2\rangle)/\sqrt{5},$$

with expressions of similar type for the remaining 13 basis functions. Despite the simple treatment of radial orbitals here, our results provide clear evidence of strong $3d$ - $4d$ intershell correlations in Cr, and suggests (by comparing energies of Tables II and III) a huge, symmetry-reversing, correlation energy in Cr of the order of 1 a.u.

For more quantitative conclusions, the radial basis set used here is too small, as is illustrated by our systematically higher energies compared to the large-basis MDHF energies in Table II. Our results constitute, however, an important step toward an accurate quantitative computation of the correlation energy. The remaining step, which lies beyond the scope of the present paper, is to combine the exact lowest symmetry subspaces delivered by our symmetry reduction algorithm

with high-accuracy, multiparameter, self-consistent radial orbital optimization routines as have been developed for Hartree-Fock theory.^{3,24,25,28}

VIII. CONCLUSIONS

We have developed and implemented an algorithm for CI calculations for atoms which allows full resolution of valence electron correlations in a large active space, via efficiently automated (and exact) symmetry reduction. Application to $3d$ transition metal atoms shows that even very small radial basis sets yield the correct qualitative picture of the electronic structure when all correlations within and between the $3d$, $4s$, $4p$, and $4d$ shells are fully resolved and when orbital exponents are optimized self-consistently for the actual CI wave functions. We trace the qualitative accuracy of our results partly to the theoretical fact that the asymptotics-based CI method used here yields the correct leading-order asymptotics for the low-lying spectral gaps in the fixed- N , large- Z limit.

In subsequent work, we aim to obtain an accurate quantitative picture, by combining the careful algorithmic treatment of correlations introduced here with suitable large-parameter orbital optimization routines as are used in (numerical or Roothaan-type) Hartree-Fock theory.

¹W. Kohn and L. J. Sham, *Phys. Rev.* **140**, A1133 (1965).

²A. Szabo and N. S. Ostlund, *Modern Quantum Chemistry* (Dover, New York, 1996).

³T. Helgaker, P. Joergensen, and J. Olsen, *Molecular Electronic Structure Theory* (Wiley, New York, 2000).

⁴D. A. Mazziotti, *Reduced-Density-Matrix Mechanics: With Application to Many-Electron Atoms and Molecules* (Wiley, New Jersey, 2007).

⁵G. Friesecke and B. D. Goddard, *Multiscale Model. Simul.* **7**, 1876 (2009).

⁶C. B. Mendl, "FermiFab Matlab/Mathematica toolbox." See <http://sourceforge.net/projects/fermifab> (2010).

⁷P.-O. Löwdin, *Phys. Rev.* **97**, 1474 (1955).

⁸G. Friesecke and B. D. Goddard, *Phys. Rev. A* **81**, 032516 (2010).

⁹D. Layzer, *Ann. Phys. (N.Y.)* **8**, 271 (1959).

¹⁰S. J. Chakravorty and E. R. Davidson, *J. Phys. Chem.* **100**, 6167 (1996).

¹¹M. P. Melrose and E. R. Scerri, *J. Chem. Educ.* **73**, 498 (1996).

¹²T. Kagawa, *Phys. Rev. A* **12**, 2245 (1975).

- ¹³J. Harris and R. O. Jones, *J. Chem. Phys.* **68**, 3316 (1978).
- ¹⁴S. Yanagisawa, T. Tsuneda, and K. Hirao, *J. Chem. Phys.* **112**, 545 (2000).
- ¹⁵C. W. Bauschlicher and P. R. Taylor, *J. Chem. Phys.* **85**, 2779 (1986).
- ¹⁶G. Friesecke and B. D. Goddard, *SIAM J. Math. Anal.* **41**, 631 (2009).
- ¹⁷A. Bunse-Gerstner, R. Byers, and V. Mehrmann, *SIAM J. Matrix Anal. Appl.* **14**, 927 (1993).
- ¹⁸P.-O. Löwdin, *J. Mol. Spectrosc.* **3**, 46 (1959).
- ¹⁹G. M. Zhislin, *Trudy Moskow Mat. Obshch.* **9**, 81 (1960).
- ²⁰J. Glimm and A. Jaffe, *Quantum Physics* (Springer, New York, 1987).
- ²¹T. Ando, *Rev. Mod. Phys.* **35**, 690 (1963); A. J. Coleman, *ibid.* **35**, 668 (1963).
- ²²P. D. Lax, *Functional Analysis* (Wiley, New York, 2002).
- ²³C. Froese Fischer, *The Hartree-Fock Method for Atoms. A Numerical Approach* (Wiley-Interscience, New York, 1977).
- ²⁴Y. B. Malykhanov and I. N. Eremkin, *J. Appl. Spectrosc.* **74**, 159 (2007).
- ²⁵C. F. Bunge, J. A. Barrientos, A. V. Bunge, and J. A. Cogordan, *Phys. Rev. A* **46**, 3691 (1992).
- ²⁶D. R. Lide, *CRC Handbook of Chemistry and Physics*, 84th ed. (CRC, Boca Raton, 2003).
- ²⁷Y. B. Malykhanov and S. A. Romanov, *J. Struct. Chem.* **46**, 204 (2005).
- ²⁸Y. Ralchenko, F.-C. Jou, D. Kelleher, A. Kramida, A. Musgrove, J. Reader, W. Wiese, and K. Olsen, *NIST Atomic Spectra Database (version 3.1.5)* (NIST, Gaithersburg, 2008).